15th World Congress on Computational Mechanics (WCCM-XV)
8th Asian Pacific Congress on Computational Mechanics (APCOM-VIII)
Virtual Congress: 31 July – 5 August 2022
S. Koshizuka (Ed.)

MODELING AND NUMERICAL SIMULATIONS OF MEMS SHUTTER DEVICES

Dominik Mayrhofer[1], **Manfred Kaltenbacher**[2]

[1] TU Graz
Inffeldgasse 18, 8010 Graz, Austria
dominik.mayrhofer@tugraz.at

[2] TU Graz
Inffeldgasse 18, 8010 Graz, Austria
manfred.kaltenbacher@tugraz.at

Key words: ADSR, MEMS, ALE, linearized flow equations

Abstract. *We investigate the acoustic behaviour of Micro-Electro-Mechanical-Systems (MEMS) with a focus on shutter devices. These shutter devices can be used for a new method of sound generation – which we call Advanced Digital Sound Reconstruction (ADSR) – where a redirection mechanism for sound pulses is incorporated [1]. With the help of this redirection mechanism, sound pulses can be generated which are superimposed to form an audio signal.*
At MEMS-scales viscous effects can play a major role regarding sound transmission. Therefore, we utilize the linearized flow equations in time domain in order to solve for the acoustic pressure while incorporating effects caused by viscous boundary layers. Furthermore, the movement of the shutter itself contributes to the overall generated sound in a negative manner. Since the generation of the sound pulses is in the ultra sound range, the generated noise by the shutter might lead to adverse effects on the human body [2]. Hence, modeling the shutter noise and understanding its generation process can help to improve the design. To model the noise generated by the shutter, we apply the arbitrary Lagrangian-Eulerian (ALE) framework to the linearized flow equations to be able to compute the noise generation on the moving geometry. The geometry update itself is governed by an artificial quasi-static mechanical problem which is solved in each step to get the new element deformation [3].
Assuming that the impact of the acoustic pressure is negligible, a simple forward coupling from the quasi-static mesh-smoothing to the the linearized flow equations is employed. Furthermore, we use a direct coupling approach to couple the acoustic wave equation to the linearized flow equations. The final coupled system is then used to characterize the impact of the shutter movement on the overall system behaviour of a certain embodiment.

1 Introduction

In this manuscript a shutter device based on Micro-Electro-Mechanical-Systems (MEMS) technology is investigated. The modeling strategy for a particular valve based on the patent [4] revolves around its usage for a new method of sound generation which we call Advanced Digital Sound Reconstruction (ADSR) [5]. This method relies on the redirection of sound pulses with e.g. shutter devices which require the consideration of multiple effects on the micro-scale. Besides standard acoustic wave propagation it is important to incorporate viscous effects which will act on the wave passing through the narrow gaps

of the shutter device. Furthermore, the shutter itself exhibits comparably large deformations which act on the acoustic paths through the valve, hence, incorporating the computation on moving domains is crucial. Based on previous investigations of the valve in [6], where a mechanical model was derived for this particular embodiment, we present an iterative modeling strategy utilizing the linearized conservation equations including viscous effects on moving domains.

2 Modeling strategy

For the investigations of shutter devices used for ADSR it is often times applicable to not fully model the contact problem since full contact is not necessary for the operating principle from an acoustic point of view. Instead it is enough, that the air passage is small enough so that viscous effects effectively act as a sealing. In literature a wide variety of methods dealing with moving domains for the mixed wave equation up to the full Navier-Stokes equations is available [7, 8, 9, 10, 11]. Due to the nature of the underlying problem – where taking the contact into account is not a necessity – an Arbitrary Lagrangian-Eulerian (ALE) approach has been used.

2.1 ALE-framework for viscous acoustics

Based on the conservation of mass - and momentum in ALE-formulation given in [12], the linearized conservation equations in ALE-formulation can be derived with a perturbation ansatz. Furthermore, using the adiabatic relation between pressure and density [13] finally leads to

$$\frac{1}{\rho_0 c_0^2}\frac{\partial p}{\partial t} + \nabla \cdot \boldsymbol{v} - \frac{1}{\rho_0 c_0^2}\boldsymbol{v}_\mathrm{g} \cdot \nabla p = 0 \tag{1}$$

for the conservation of mass as well as

$$\rho_0 \frac{\partial \boldsymbol{v}}{\partial t} - \rho_0 \boldsymbol{v}_\mathrm{g} \cdot \nabla \boldsymbol{v} = \nabla \cdot [\boldsymbol{\sigma}] \tag{2}$$

for the conservation of momentum, where the fluid stress tensor $[\sigma]$ is given by

$$[\sigma] = -p\,[\boldsymbol{I}] + \mu_\mathrm{f}(\nabla \boldsymbol{v} + (\nabla \boldsymbol{v})^\mathsf{T}) - \frac{2}{3}\mu_\mathrm{f}(\nabla \cdot \boldsymbol{v})\,[\boldsymbol{I}]. \tag{3}$$

In these equations ρ_0 denotes the mean density, c_0 the speed of sound, p the perturbed fluid pressure, $\boldsymbol{v}$ the perturbed fluid velocity and $\boldsymbol{v}_\mathrm{g}$ the grid velocity. Furthermore, $\boldsymbol{I}$ represents the identity tensor and μ_f the dynamic viscosity of the fluid. In (2) we already inserted the constitutive equations based on Stokes' assumptions [13]. For the sake of brevity the authors refer to the linearized conservation equations as linearized flow equations or in short LinFlow equations.

2.2 Geometry deformation

For the calculation of the deformed mesh as well as the grid velocity a quasi static solution of an artificial mechanical problem is used. Although computationally more expensive than other schemes, this approach brings additional flexibility since the mesh smoothing can be easily altered locally by making e.g. the stiffness tensor location dependent [3]. For simpler problems an artificial material constant in time and space is already sufficient which leads to

$$-\nabla \cdot \left([\boldsymbol{c}] : \frac{1}{2}(\nabla \boldsymbol{u} + (\nabla \boldsymbol{u})^\mathsf{T}) \right) = 0. \tag{4}$$

In this equation $[\boldsymbol{c}]$ denotes the stiffness tensor and $\boldsymbol{u}$ the displacement vector of the artificial mechanical problem. The grid velocity $\boldsymbol{v}_\mathrm{g}$ can be calculated based on the displacement vector and a simple BDF2 scheme [3].

2.3 Coupling strategy

When the back-coupling of the perturbed fluid-pressure on the real mechanical problem can be neglected, it is sufficient to employ a simple forward coupling strategy. Assuming that the deformation profile is known, Dirichlet boundary conditions (BCs) can be used for the calculation of the deformed mesh. Hence, the artificial mechanical problem is solved in a first step. In the next step the updated (deformed) geometry as well as the grid velocity is used to solve (1) and (2) accordingly. Since the calculation of (1) and (2) is computationally quite expensive, it is important to keep the deforming region quite small. Hence, we couple to the standard (non-ALE) version of (1) and (2) as soon as possible. The formulation for these equations is only a subset of the presented ones and can be obtained by setting the grid velocity to zero. Finally, it has to be said that the linearized conservation equations themselves also require a lot more computational effort than the standard acoustic wave equation given by

$$\frac{1}{c_0^2}\frac{\partial^2 p_\mathrm{a}}{\partial t^2} - \nabla\cdot\nabla p_\mathrm{a} = 0. \tag{5}$$

Here, the acoustic pressure p_a is the only scalar variable to be solved for. Therefore, coupling conditions regarding the continuity of surface traction

$$-p_\mathrm{a}\boldsymbol{n} = \boldsymbol{\sigma}\cdot\boldsymbol{n} \tag{6}$$

as well as continuity of normal acceleration

$$\frac{\partial \boldsymbol{v}}{\partial t}\cdot\boldsymbol{n} = -\frac{1}{\rho_0}\nabla p_\mathrm{a}\cdot\boldsymbol{n} \tag{7}$$

are employed similarly to [6]. Here, $\boldsymbol{n}$ denotes the outward facing normal vector of the LinFlow domain. Since the acoustic wave equation is also solved on an undeformed domain, we can simply couple it directly to the linearized conservation equation, thus, minimizing computational effort.

3 Model setup

The presented framework has been applied to model and simulate an electrostatic valve based on the patent [4]. The general structure of this valve can be seen in Fig. 1. The simulation itself is split into two parts due to its complexity. In a first step, the presented ALE-framework is used to determine the acoustic response of the valve. Here, an axi-symmetric model with effective hole diameters are used in order to keep the computational effort reasonable. In a second step, the acoustic response of the valve is surface averaged and applied to the second purely acoustic propagation model which represents the measurement setup.

3.1 Valve model

Regarding the model of the valve the real geometry has been used to construct an effective 2D axi-symmetric model. Since we focus on the propagated sound, the most important factor for the effective

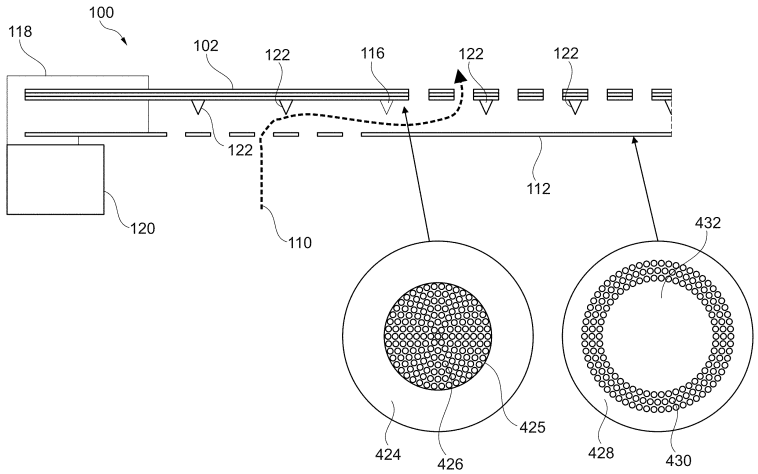

Fig. 4

Figure 1: Structure of the investigated valve. Two inversely perforated back plates with a small gap in between allow the sound to pass through. When a voltage is applied, the electrostatic force pulls the plates together and effectively seals the acoustic path [4].

2D model is the surface area. Hence, the 2D model is tuned to have equal radially averaged area leading to an equivalent perforation grade for the 2D and 3D model. Due to this averaging, the hole size is altered leading to differences in the interaction of the two plates as well as the viscous dissipation. The difference regarding the interaction of the plates would be the result of a different pressure build-up between the plates. By imposing the displacement and neglecting the back-coupling, we also effectively suppress this negative effect with the chosen modeling approach. Regarding the different hole size and the inherent influence regarding the viscous effects we assume that this effect is negligible. The reason for this is that the effective lengths responsible for dissipating acoustic energy are very low. Furthermore, the sound radiated from the movement of the back-plates is mainly influenced by the actual area – which has been prioritized. Additionally it has to be said that locally the Knudsen number can get comparably high which would violate continuum theory [14]. Similar to before though, the effect is negligible for this case – mainly the deforming shutter in combination with the accompanying change of impedance is of importance.

3.1.1 Simulation setup

The model for the ALE-based computation can be seen in Fig. 2. The center region denoted as LinFlow (ALE) is the model of the valve itself including some surrounding air where the LinFlow equations in ALE-formulation are solved. In order to ensure that only a fully developed flow field is coupled to the acoustic wave equation, an additional LinFlow region called LinFlow (undeformed) is used where no geometry update is considered. Afterwards, non-conforming interfaces are used to couple to the propagation domains Propagation 1 and Propagation 2 where only the acoustic wave equation is solved. Finally, the propagation domains are terminated with a perfectly matched layer (PML) to model free radiation. Regarding boundary conditions we prescribe the displacement for the bottom back plate (BBP) directly on Γ_{BBP} and for the top back plate (TBP) on Γ_{TBP}. The outer boundaries combined in Γ_{fix} of the

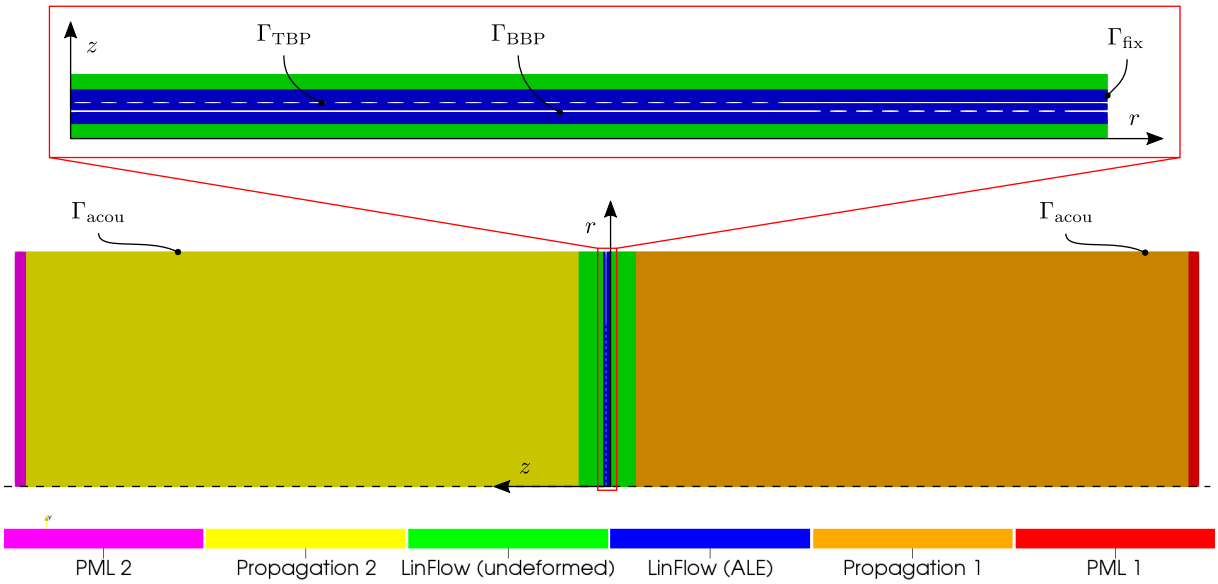

Figure 2: Model of the axi-symmetric valve where the positive z-direction points towards the measurement channel used for the subsequent propagation simulation. At both ends a perfectly matched layer (PML) has been used to model free radiation. Besides the prescribed velocity at the boundaries due to the deformation, no-slip BCs have been used for the LinFlow domain. The acoustic domain features natural sound hard boundary conditions.

blue region are simply fixed. For the linearized conservation equations we prescribe the velocity at Γ_{BBP} and Γ_{TBP} wheres the rest of the boundaries are equipped with no-slip BCs. For the regions Propagation 1 and Propagation 2 we only use natural sound hard boundary conditions on all boundaries Γ_{acou} except for the coupling surfaces where we couple to the LinFlow equations or to the PML region.

3.1.2 Excitation

For the ALE-based model the displacement of the membrane has been prescribed analytically. The basis for this has been presented in [6] where a one degree of freedom (1-DOF) model was used to accurately model the displacement of the back plates. This model includes non-linearties based on the electrostatic force but also caused by non-linear stiffness as well as squeeze film damping based on models presented in [15] and [16] respectively. It has to be noted that the actual deflection profile has been calculated by a mixture of measurements of the actual valve as well as shape measurements of a slightly different device from [17]. Combining the center displacement and the shape function interpolator introduced in [6], the overall displacement assuming axisymmetric deformation can be calculated. With this approach, the back-coupling of the pressure build-up is inherently incorporated. The center displacement based on the 1-DOF compared to the measured center displacement of the actual actuator can be seen in Fig. 3a. For the analytical description of the shape function of the back-plate the results from [6] have been fitted to analytical functions. The analytical function prescribing the deflection profile is given by

$$w(t,r) = w_{\mathrm{cent}}(t)\left(f_{\mathrm{c}}(r) + f_{\mathrm{d}}(r)c_{\mathrm{d}}(t)\left(1-\exp\left(\frac{10(a-r)}{a}\right)^{-1}\right)\right) \tag{8}$$

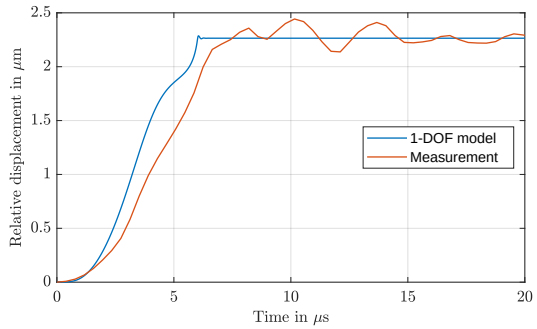

(a) Comparison of the measured and simulated center deflection based on the 1-DOF model [6].

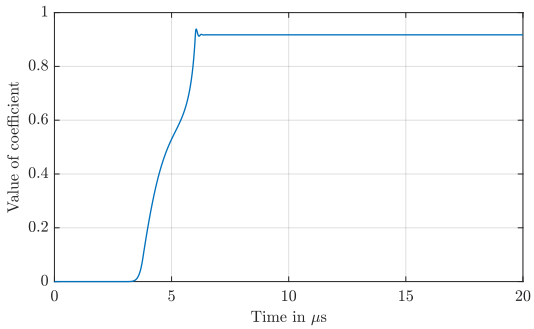

(b) Value of the time dependent weighing factor $c_\mathrm{d}(t)$ representing the weight of $f_\mathrm{d}(r)$.

Figure 3: Excitation signals used for the analytical prescription of the shutter deflection. The displacement is shown for the BBP – for the TBP a simple scaling factor is used as shown in [6].

In this equation $w(t,r)$ is the deflection profile and $w_\mathrm{cent}(t)$ the center displacement of the back plate as seen in Fig. 3a for the BBP. Furthermore, t represents time, r the radius in terms of a function and a the actual value of the radius of the valve. The base curvature function f_c as well as the deviation function f_d are fitted to the measurement data and represented by simple polynomial functions of order o in the form

$$f(r) = \sum_{i=0}^{o} a_i \left(\frac{r}{a}\right)^i, \tag{9}$$

where the coefficients are given in Tab. 1. The time dependent weighting factor $c_\mathrm{d}(t)$ has also been fitted to measurements and can be seen in Fig. 3b. It can be clearly seen from Fig. 3b that the deviation of

Table 1: Coefficients for the polynomial representation of f_c and f_d

	f_c	f_d
a_0	1.00086252e+00	-2.01446299e-03
a_1	-7.55222479e-02	2.84258704e-01
a_2	1.97804624e+00	-9.95036852e+00
a_3	-2.27194589e+01	1.30675137e+02
a_4	9.86336712e+01	-7.94195752e+02
a_5	-2.36089945e+02	2.64045851e+03
a_6	3.09304956e+02	-4.99587778e+03
a_7	-2.09088868e+02	5.34844701e+03
a_8	5.70566097e+01	-3.01786134e+03
a_9	-	6.98031551e+02

the initial shape is zero at the beginning and increases sharply over time. Since according to Fig. 3a increasing time corresponds to increasing deflection, the influence of non-linearities plays a major role for larger deflection. Figure 4 shows the normalized shape functions of the back plates in their final position where the effect of the non-linear deflection profile can be clearly seen.

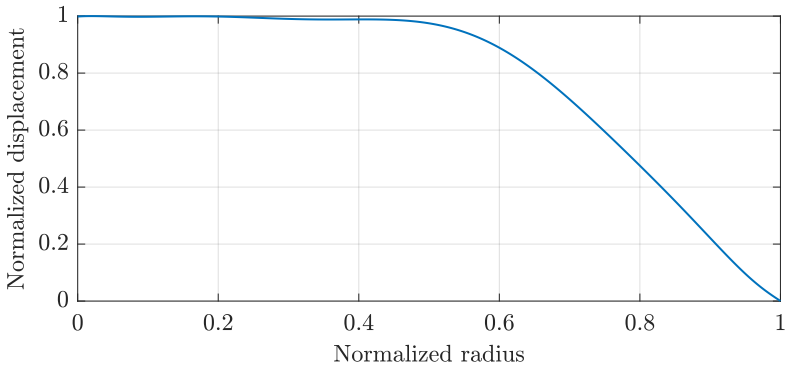

Figure 4: Normalized shape function of the back plates for $t \to \infty$.

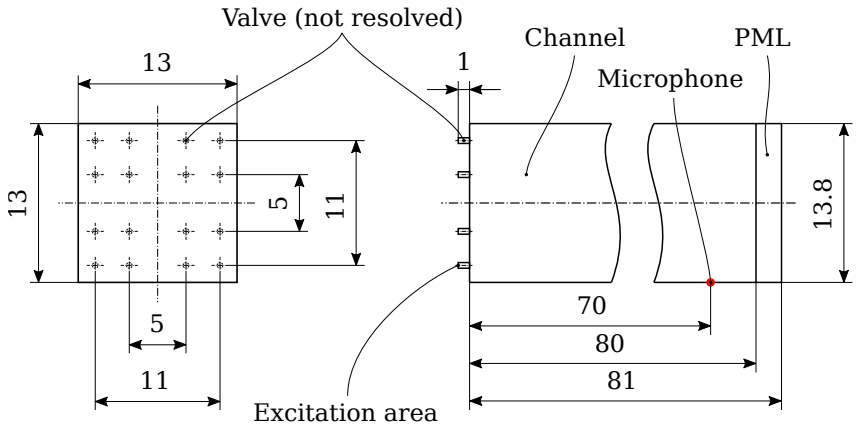

Figure 5: Simplified propagation model used for comparison to the measurements (dimensions given in mm). The model features 16 valve-channels, where the individual valves are not resolved but replaced by an effective normal velocity boundary condition. The mesh supports frequencies up to 200 kHz [6].

3.2 Propagation model

For the comparison of the model results to the measurements an additional simplified propagation model has been used. Similar to [6] an effective velocity is used as a boundary condition to excite the system. The propagation model used can be seen in Fig. 5. The effective normal velocity used for the boundary condition has been calculated based on the results from the ALE-model, where the acoustic particle velocity of the channel has been evaluated and surface averaged via

$$v_{\mathrm{eff,ALE}}(t) = \frac{2\pi \int_0^a v_{\mathrm{a,ALE}}(t,r)\, r \,\mathrm{d}r}{a^2\pi} \tag{10}$$

This strongly suppresses radial modes and alters the results but can be justified for this application. First of all, since the mesh only supports frequencies up to 200 kHz, all radial modes would not be resolved by the mesh anyway. This also applies to the measurements where frequencies up to only 100 kHz are supported. Additionally, the radial modes start just right before the contact where the electrostatic force

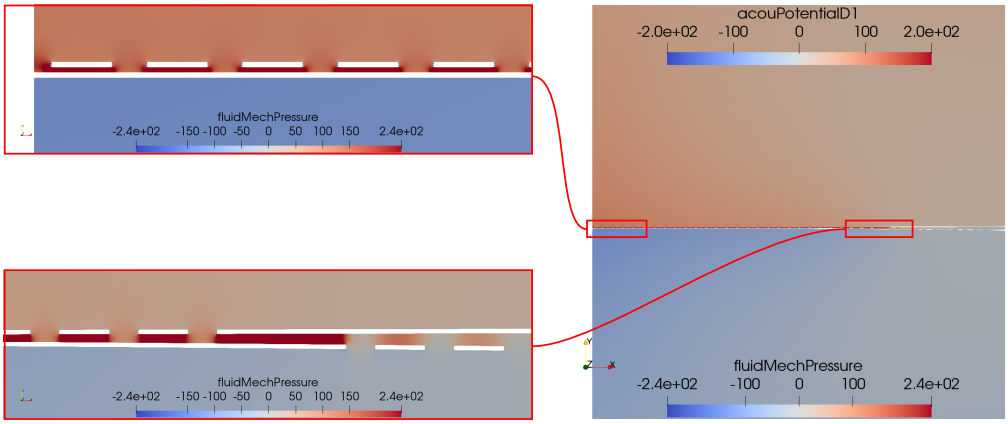

Figure 6: Snapshot of the axi-symmetric ALE-based computation. The two close-ups show the different pressure distribution at the symmetry axis as well as in between where the perforation switches.

is so strong, that an additional acceleration peak can be observed for the plate deflection. Since the model is inherently deviating from the measurements after the contact due to the fact, that the oscillation of the two plates after the snap-in is not represented in the 1-DOF model. Hence, the influence on the representative time which can be used for comparison to the measurements will be negligible.

4 Simulation results

Based on the presented model the simulation results for the ALE-based computation as well as the propagation model are presented. All simulation results have been obtained with our in-house open source FEM-solver *openCFS* [18].

4.1 ALE

Regarding the ALE-based computation an exemplary field result is shown in Fig. 6. Here it can be seen that the wave propagation through the different computation domains (LinFlow ALE, LinFlow non-ALE and acoustic) is working well. Furthermore, the LinFlow equations enable solving the closing process of the valve accurately. As shown in the close-ups, the pressure distribution is highly dependent on the actual local velocity of the plates. Since they vary strongly due to the highly non-linear electrostatic forcing as well as the squeeze film damping incorporated in the 1-DOF model, the pressure distribution varies locally. Up to about 5 µs the influence is not that strong, but the second velocity peak stemming from the snap-in effect introduces strong locally varying velocity profile. The main reason for these local differences is that the center of the back plate gets flattened when getting close to contact – as seen in Fig. 4. Hence, at some point the acceleration over the diameter will increase for larger values of r, resulting in the local variation of the velocity inducing radial modes. As previously mentioned the effective velocity has been calculated by surface averaging the acoustic particle velocity. The resulting effective particle velocity as well as the filtered one suitable for the propagation grid can be seen in Fig. 7. This plot shows that the radial modes excited by the locally varying velocity profile are of very high frequency which are filtered out due to the fact that they could not be measured with the used measurement setup.

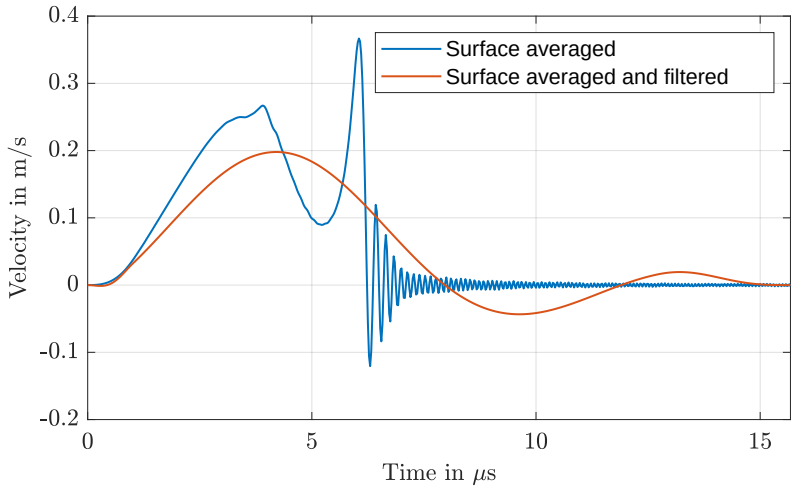

Figure 7: Comparison of the surface averaged velocity to the surface averaged and filtered version used for the propagation model. The upper frequency for the filtering stage was set to 140 kHz.

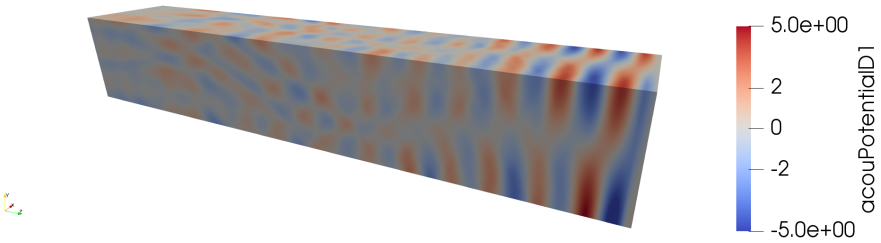

Figure 8: Snapshot of the first time derivative of the acoustic potential denoted as acouPotentialD1 at the time $t = 250\,\mu$s. The propagation direction is from left to right and only four of the overall 16 valves have been excited. Although the input velocity has already been filtered, the sound field is quite complex and features longitudinal as well as transversal modes.

4.2 Propagation

Applying the surface averaged and filtered particle velocity show in Fig. 7 and using it as an inhomogeneous boundary condition for the propagation model from Fig. 5 gives us the acoustic response of the valve during the closing process. For the simulation at hand, only four of the overall 16 valves have been excited. Since the model is symmetric and linear, the resulting sound pressure at the microphone position shown in Fig. 5 can be calculated by superposition. The advantage of this approach is that the excitation of just one or multiple groups can be investigated. The resulting sound pressure at $t = 250\,\mu$s can be seen in Fig. 8. For the evaluation of the results at the microphone position it has to be noted, that the time signal was filtered afterwards to match the filtering conditions of the measurement process where a B&K Nexus Conditioning Amplifier was used. Hence, the final filtering stage features a Butterworth filter of second order with 1 dB attenuation at 100 kHz. Finally, the obtained simulation result compared to the measurement can be seen in Fig. 9. The results show that the initial peaks are captured very well.

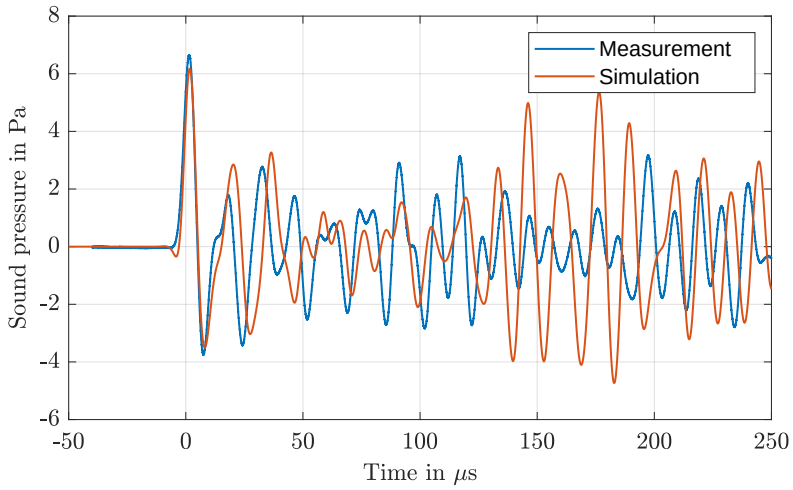

Figure 9: Comparison of the measured- and modeled sound pressure at the microphone position.

Afterwards, deviations from the measurement signal occur, which is to be expected since the combined oscillation of the back plates snapping together is not modeled in the simplified mechanical model that has been used for the prescription of the movement.

5 Conclusion

An iterative solving process based on solving the linearized conservation of mass - and momentum equations of a compressible fluid in an ALE-framework coupled to the acoustic wave equation has been presented. We have shown that already an axi-symmetric ALE-based model utilizing equal radially averaged surface areas in combination with a fitted plate deflection model is enough to accurately model the highly non-linear process of closing the valve in snap-in mode. Based on the results of the 1-DOF model presented in an earlier publication the ALE-model has been impinged with these displacement boundary conditions, implicitly modeling the contact problem. Furthermore, the solution of the ALE-model has been successfully applied to the propagation model in a simple forward coupling step and compared to measurements. The comparison of the results have shown good agreement with expectations as well as the measurements verifying the proposed solution strategy.

REFERENCES

[1] Mayrhofer, D. and Kaltenbacher M. Investigation of a new method for sound generation – Advanced Digital Sound Reconstruction. *e & i Elektrotechnik und Informationstechnik*. (2021) **138.3**: 148–154.

[2] Smagowska, B. and Małgorzata, P. L. Effects of Ultrasonic Noise on the Human Body – A Bibliographic Review. *International Journal of Occupational Safety and Ergonomics* (2013) **19:2**: 195-202.

[3] Link, G., Kaltenbacher, M., Breuer M. and Döllinger, M. A 2D finite-element scheme for fluid–solid–acoustic interactions and its application to human phonation. *Computer Methods in Applied Mechanics and Engineering*. (2009) **198**: 3321-3334.

[4] Manz, J., Klein, W. and Tumpold, D. *Photoacoustic Sensor Valve*. U.S. Patent and Trademark Office, U.S. Patent Application No. 20200319144, (2020)

[5] Mayrhofer, D. and Kaltenbacher M. A New Method for Sound Generation Based on Digital Sound Reconstruction. *Journal of Theoretical and Computational Acoustics*. (2021) **29:04**

[6] Mayrhofer, D. and Kaltenbacher M. Transmission behaviour and noise generation of MEMS shutter devices. DAGA - 48th German Annual Conference on Acoustics (2022), 1346-1349

[7] Guasch, O., Arnela, M., Codina, R. and Espinoza, H. A Stabilized Finite Element Method for the Mixed Wave Equation in an ALE Framework With Application to Diphthong Production. *Acta Acustica united with Acustica*. (2019) **102**: 94-106

[8] Stockie, J.M., Mackenzie, J.A. and Russell, R.D. A Moving Mesh Method for One-dimensional Hyperbolic Conservation Laws. *SIAM Journal on Scientific Computing*. (2001) **22**: 1791-1813

[9] Wall, W.A., Gerstenberger, A., Gamnitzer, P., Förster, C. and Ramm, E. Large Deformation Fluid-Structure Interaction – Advances in ALE Methods and New Fixed Grid Approaches. *Fluid-Structure Interaction. Lecture Notes in Computational Science and Engineering*. Springer, Berlin, Heidelberg, Vol. 53., (2006)

[10] Schott, B., Ager, C. and Wall, W.A. Monolithic cut finite element–based approaches for fluid-structure interaction. *International Journal for Numerical Methods in Engineering*. (2019) **119**: 757-796

[11] Tang, H. A moving mesh method for the Euler flow calculations using a directional monitor function. *Communications in Computational Physics*. (2006) **1**:656-676

[12] Donea, J., Huerta, A., Ponthot, J.-Ph. and Rodríguez-Ferran, A. Arbitrary Lagrangian–Eulerian Methods. *Encyclopedia of Computational Mechanics*. John Wiley & Sons, Ltd, (2004)

[13] Kaltenbacher, *M. Numerical Simulation of Mechatronic Sensors and Actuators: Finite Elements for Computational Multiphysics*. Springer, 3rd edition, (2015)

[14] Hadjiconstantinou, N.G. The limits of Navier-Stokes theory and kinetic extensions for describing small-scale gaseous hydrodynamics. *Physics of Fluids* (2006) **18:11**

[15] Wygant, I.O., Kupnik, M., and Khuri-Yakub, B.T. Analytically calculating membrane displacement and the equivalent circuit model of a circular CMUT cell. 2008 IEEE Ultrasonics Symposium (2008), 2111-2114

[16] Bao, M., Yang, H., Sun, Y. and Wang, Y. Squeeze-film air damping of thick hole-plate. *Sensors and Actuators A: Physical*. (2003) **108**: 212-217

[17] Tumpold, D. and Kaltenbacher, M. Precise numerical simulation of electrostatically driven actuators with application to MEMS loudspeakers. ENOC 2014 - Proceedings of 8th European Nonlinear Dynamics Conference (2014)

[18] Kaltenbacher, M. *openCFS*. `https://www.opencfs.org`, ver. 22.02 (2022)